Revista de Metalurgia
October–December 2018, 54 (4), e131
ISSN-L: 0034-8570
https://doi.org/10.3989/revmetalm.131

A further study of the kinetics of recrystallization and grain growth of cold rolled TWIP steel

Fernando de las Cuevas[a,b,✉], Claudio Aguilar[c], Javier Gil Sevillano[d]

[a]UPNA (Universidad Pública de Navarra), Campus de Arrosadia, Dpto. de Ciencias, 31006 Pamplona, Spain
[b]SIEMENS GAMESA Renewable Energy, S.A, Avda. Ciudad de la Innovación 2, 31621 Sarriguren, Navarra, Spain
[c]USM (Universidad Técnica Federico Santa María), Dpto. de Ingeniería Metalúrgica y Materiales, Av. España 1680, Valparaíso, Chile
[d]CEIT y TECNUN (Universidad de Navarra), M. Lardizábal 15, 20018 San Sebastián, Spain

(✉Corresponding Author: fernando.delascuevas@unavarra.es)

Submitted: 13 March 2018; Accepted: 11 June 2018; Available On-line: 2 Octubre 2018

ABSTRACT: Hot rolled, laboratory-cast, TWIP steel specimens with composition 22% Mn-0.6% C (in mass %) was cold rolled to reductions of 40%, 50%, 60% and 70% and afterwards isothermally annealed for various times in the interval of temperatures 450 ºC ≤ T ≤ 1100 ºC. The purpose was to study the precipitation behavior and its plausible effect in the static recrystallization and grain growth kinetics. Two types of precipitates were found in 600 °C ≤ T ≤ 700 °C for long times: (Fe, Mn)$_3$C – Cementite and Vanadium Carbonitrides. Recrystallized grain size was very fine, D_0 ≤ 2 μm. Also, a weaken retained rolling texture in the recrystallisation process was found. Calculated value of activation energy for recrystallization, Q_{soft} = 281 ± 70 kJ·mol^{-1} was obtained which corresponds practically with the activation energy for bulk self-diffusion in austenite (270 kJ·mol^{-1}) and for *Mn* diffusion in the austenite lattice (265 kJ·mol^{-1}). Nevertheless, higher calculated activation energy for grain growth, Q_{GG} = 384 ± 60 kJ·mol^{-1} was found with a grain growth exponent of n_{GG} ~ 4. Consequently, the most plausible explanation is that the quantity of precipitates is enough to have relevant pinning effect of migrating grain boundaries during grain growth due to the mean length between precipitates, L_{prec}, is smaller than some threshold value of grain size, $L_{prec} < D_{threshold}$, being, $D_0 << D_{threshold}$.

KEYWORDS: Activation energy; Cold rolled; Grain growth; Grain growth exponent; Isothermal annealing treatments; Precipitation; Static recrystallization; Texture; TWIP steel

Citation/Citar como: de las Cuevas, F.; Aguilar, C.; Gil Sevillano, J. (2018). "A further study of the kinetics of recrystallization and grain growth of cold rolled TWIP steel". *Rev. Metal.* 54(4): e131. https://doi.org/10.3989/revmetalm.131

RESUMEN: *Un estudio adicional de la cinética de recristalización y crecimiento de grano del acero twip laminado en frío.* Muestras de acero TWIP laminadas en caliente en laboratorio de composición, 22% de Mn, 0,6% de C (% en masa) se laminaron en frío a reducciones de 40%, 50%, 60% y 70% para recocerlas isotérmicamente en el intervalo de temperatura 450 ºC ≤ T ≤ 1100 ºC. El objetivo fue estudiar la precipitación y su efecto razonable en la recristalización estática y cinética de crecimiento de grano. Se encontraron dos tipos de precipitados en 600 ºC ≤ T ≤ 700 ºC a tiempos largos de recocido: (Fe, Mn)$_3$C – Cementita y Carbonitruros de Vanadio. El tamaño de grano recristalizado fue muy fino D_0 ≤ 2 μm. Además, se encontró que la textura de laminación se hereda en la recristalización muy debilitada. La energía de activación para la recristalización calculada fue Q_{soft} = 281 ± 70 kJ·mol^{-1} que se corresponde prácticamente con la energía de activación para la autodifusión en austenita (270 kJ·mol^{-1}) y para la difusión del *Mn* en austenita (265 kJ·mol^{-1}). Sin embargo, la energía de activación de crecimiento de grano obtenida fue significativamente mayor Q_{GG} = 384 ± 60 kJ·mol^{-1} con un exponente de crecimiento de grano, n_{GG} ~ 4. Consecuentemente, la explicación más razonable es que la cantidad de precipitados es suficiente para tener un efecto de fijación en la migración de las juntas de grano durante el crecimiento debido a que la longitud media entre precipitados, L_{prec}, es menor que algún valor umbral de tamaño de grano, $L_{prec} < D_{umbral}$, siendo $D_0 << D_{umbral}$.

PALABRAS CLAVE: Acero TWIP; Crecimiento de grano; Energía de activación; Exponente de crecimiento de grano; Laminado en frío; Precipitación; Recristalización estática; Textura; Tratamientos de recocido isotermos

ORCID ID: Fernando de las Cuevas (https://orcid.org/0000-0002-2344-7353); Claudio Aguilar (https://orcid.org/0000-0002-9013-5835); Javier Gil Sevillano (https://orcid.org/0000-0002-1716-8200)

1. INTRODUCTION

Over last decades, the twinning - induced plasticity Fe-Mn-C (TWIP) steels have been the focus on huge amount of research works due to their prominent strength – ductility compounding which develops from the occurrence of extended mechanical twinning during plastic deformation under mechanical loads (Grässel and Frommeyer, 1998; Frommeyer *et al.*, 2000; Cornette *et al.*, 2005; Scott *et al.,* 2006; Bouaziz *et al.,* 2008; Hamada *et al.*, 2010; Bouaziz *et al.,* 2011; De Cooman *et al.*, 2011; Galán *et al.*, 2012; Gil Sevillano and De las Cuevas, 2012; Chen *et al.*, 2013; De las Cuevas *et al.*, 2014; Ghasri-Khouzani and McDermid, 2015; Pierce *et al.*, 2015; De las Cuevas and Gil Sevillano, 2017).

In TWIP steels, the fully austenitic microstructure can be retained by means of high level alloying with elements such as *Mn*, *Al* and *Si*. *Al* and *Si* are mainly used to adjust the magnitude of the stacking fault energy, γ_{SFE}, of austenite (Frommeyer *et al.*, 2000). Furthermore, they also strengthen the steel by solid solution hardening and stabilize austenite owing to their ability of slowing down the precipitation of carbides, especially cementite, leaving more carbon available for the enrichment of austenite (Leslie and Rauch, 1978).

Additions of *Al* generally increase γ_{SFE}, whilst *Si* is reported to lower it at concentrations approximately ≥ 4 wt%, Schramm and Reed (1975), but to increase it at lower concentrations (Dumay *et al.*, 2008). Then, by adjusting the chemical composition and controlling the carbon concentration, the austenitic structure is maintaned; the emergence of α'*- martensite* (*BCC*) and ε*– martensite* (*HCP*) are inhibited and can conduct to prominent mechanical properties by TWIP effect, (Grässel *et al.*, 1997; Grässel *et al.*, 2000; Allain *et al.*, 2004), leading to a dynamic Hall-Petch effect as the deformation proceed (De las Cuevas *et al.*, 2010a). It is widely recognized that the TWIP effect occurs in a stable austenite with γ_{SFE} approximately of 25 $mJ{\cdot}m^{-2}$ (Frommeyer and Grässel, 1998). More recent research works on this relevant point, Pierce *et al.* (2014) has thrown more detailed aspects of the deformation mechanism, phase stability and stacking fault energy in TWIP steels.

In a previous work developed by De las Cuevas *et al.* (2010b), the static recrystallization and grain growth kinetics in a 22% Mn, 0.6% C (mass %) TWIP steel were studied. The present research work aims to obtain further data of the isothermal annealing behavior in TWIP steel to formulate any industrial application of this material since the desired compounding of elastic limit and tensile strength required for a specific application involves an unchanging austenitic structure with a preset grain size. Therefore, a thorough characterization of the precipitation in the interval of temperature 600 °C ≤ T ≤ 900 °C and its arguable effect in the static recrystallization and grain growth kinetics were studied in detail. With all the data obtained, a refined characterisation of the kinetic equation of recrystallization and grain growth for 60% cold rolled TWIP steel was performed to obtain the activation energy for both recrystallization and grain growth. Finally, textural evolution via X-ray of isothermal treatments of cold rolled TWIP steel at different stages: recrystallized structure (without apparent grain growth), and recrystallized plus grain growth with different grain sizes structures was characterized.

2. MATERIAL AND EXPERIMENTAL PROCEDURES

Hot rolled samples (5.4 mm thick) of TWIP steel with composition depicted in Table 1 were reduced by cold rolling at laboratory mill to different thicknesses, R: 3.24 mm (R = 40%), 2.70 mm (R = 50%), 2.16 mm (R = 60%) and 1.60 (R = 70%) and subsequently isothermally annealed. The annealing treatments were performed in a salt bath furnace in the interval of temperature 450 °C ≤ T ≤ 900 °C and they were interrupted by quenching water after different annealing times ranging 1 s ≤ t ≤ 43740 s. In a similar manner annealing treatments at 1000 ºC and 1100 ºC were carried out in a resistance furnace under Ar protective atmosphere in order to avoid decarburation of the steel, De las Cuevas and Gil Sevillano (2017), followed by water quenching too. The heating time was controlled by treating dummy samples with inserted thermocouples. The evolution of recrystallisation and grain growth was followed by control of the softening kinetics complemented by metallographic and EBSP-OIM observations. The samples were analysed using a Philips XL30 SEM microscope equipped with a TSL module for automatic EBSP acquisition. The grain sizes of the specimens were measured as the mean linear intercept using OIM-EBSP images. Further experimental points are described (De las Cuevas

TABLE 1. Chemical composition of TWIP steel

	Chemical composition (% in mass)							
Material	**Fe**	**C**	**Mn**	**Si**	**N**	**S**	**P**	**Nb**
TWIP Steel	Bal.	0.59	22.30	0.22	-	-		-

et al., 2010b). These annealing treatments provided equiaxed grain sizes after complete recrystallization and grain growth in the interval of 1.50 μm ≤ D < 50 μm.

The development of macro-texture was performed by X-ray diffraction in a Philips Xpert diffractometer. The selected specimens to study the evolution of macro-texture were: cold rolled 60%, recrystallized structure (neglected grain growth) with 1.50 ± 0.02 μm of grain size, and recrystallized plus grain growth structures with 12.2 ± 0.3 μm and 35 ± 1 μm.

In order to detect fine precipitates in the annealed samples, single stage carbon extraction replicas were prepared using the conventional method starting from surfaces prepared as for optical microscopy. Afterwards a selective electrolytic dissolution method to remove the matrix around the carbides was used (Marder, 1989). The extracted carbon replicas were examined using a Jeol JEM 200CX (STEM) electron microscope operated at 200 kV.

3. RESULTS

3.1. Softening kinetics

Owing to the industrial importance of 60% reduction, thorough characterization of the isothermal annealing behaviour after such reduction was carried out. Figure 1 shows the mean value of hardness (HV) versus annealing time (t) for reduction R = 60% TWIP cold rolled specimens. The dashed black line corresponds to the Vickers Hardness at 60% cold rolled structure, HV_{CR} = 506 ± 3 kgf•mm^{-2}. The softening kinetics was very similar for the four reductions.

First of all, the effect of annealing at 450 ºC was very weak. There was a small initial hardening after the shortest annealing. The shortest annealing corresponded to 1 s, but in fact it took about 8 s to reach the 450 ºC temperature. Thereafter an almost negligible softening took place. A weaker hardening at the start of the annealing was only perceptible at 600 ºC or 650 ºC. This initial hardening did not appear anymore for higher treatment temperatures. This stage of static strain ageing (SSA), is well known attributable to solid solution segregation at pre-existing dislocation lines (Vidoz *et al.*, 1963). Figure 2 illustrates the transient static strain ageing stage of initial hardening (ΔHV_i) at 450 ºC and 600 ºC as a function of level reduction.

At 600 ºC and 650 ºC the hardness evolution with time pointed typicallly the sigmoidal shape of recrystallisation softening. At high times some contribution of grain growth will also take place, but microstructural characterisation shows that grain growth is very slow at such temperatures. For 600 ºC, recrystallization is not completed for the maximum time verified (12.5 hours), the fraction recrystallized

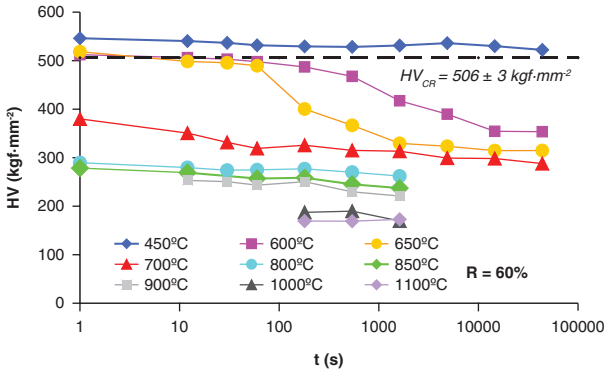

FIGURE 1. Vickers Hardness vs. logarithm of annealing time for reduction R = 60% cold rolled TWIP steel. Annealing temperature in the interval of 450 ºC ≤ T ≤ 1100 ºC.

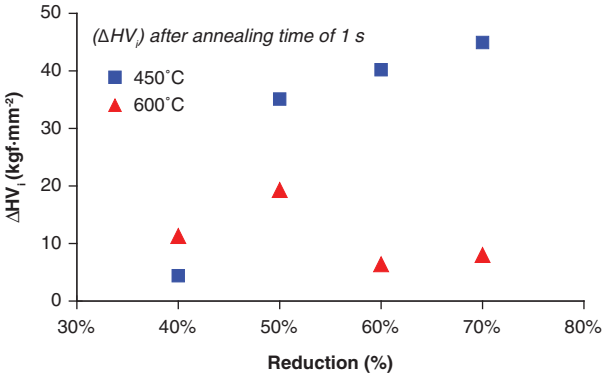

FIGURE 2. Transient hardening stage at the beginning of the annealing treatments at 450 ºC and 600 ºC in TWIP steel.

being known from the metallographic observations, $[X_{sof}(t = 12.5\ h)]_{600ºC} \approx 87\%$ as it is depictied in Fig. 3.

At 700 ºC the hardness evolution with time showed less clearly the sigmoidal shape of recrystallisation softening. Judging by the final hardness values obtained after 12.15 h at 600 ºC and 700 ºC, the influence of the cold rolling reduction (from 40% to 70%) in the recrystallised grain size was small. Figure 4 illustrates such small influence at both temperatures. In addition, it was confirmed by metallographic examination, that the grain sizes of this steel after static recrystallisation are very small, in agreement with the results reported (Scott *et al.*, 2006; De las Cuevas *et al.*, 2010b).

Finally, from 800 ºC to 1100 ºC, the softening curves in all their time range correspond to the lower arm of their sigmoidal shape and, in fact, to grain growth. Hardness shows an approximately exponential decrease with time. This meant that in less than one second, recrystallisation was complete at T ≥ 800 ºC. These results were complemented with microstructural observations that confirm this recrystallization and grain growth behaviour.

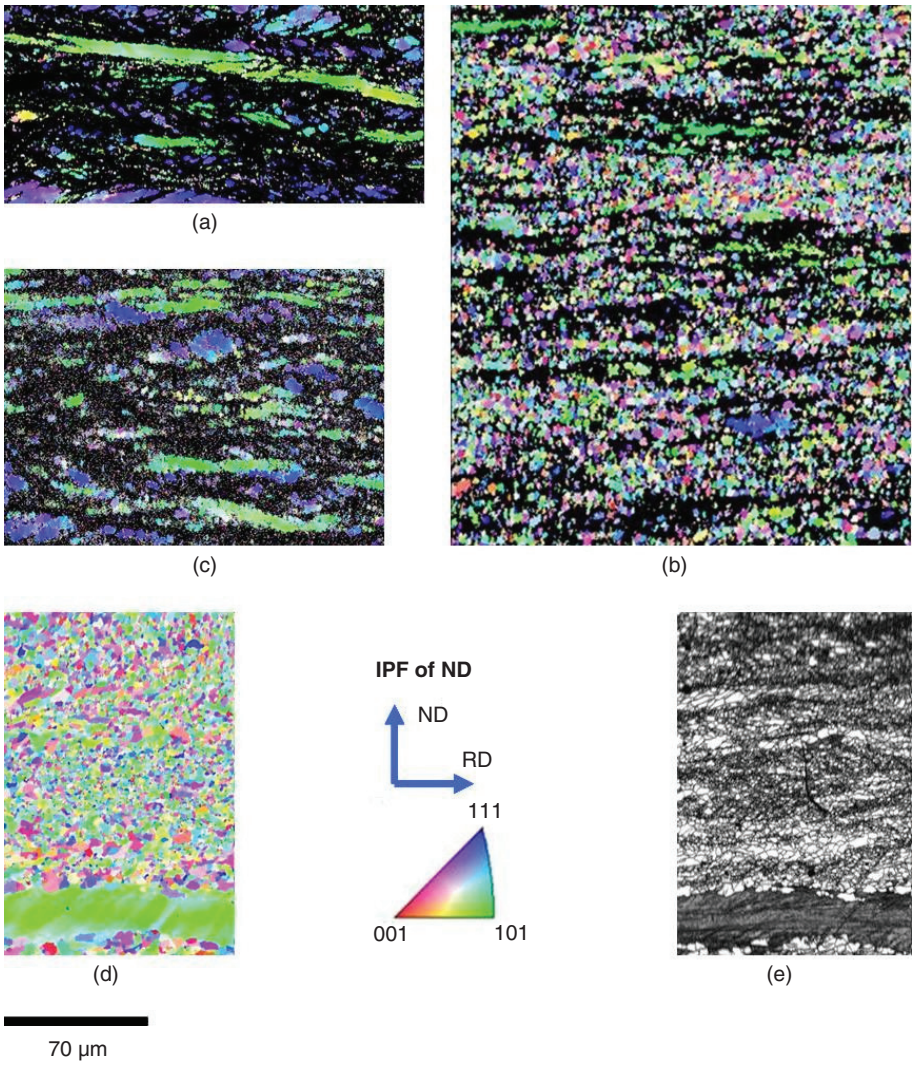

FIGURE 3. Evolution of recrystallization of the 60% cold rolled TWIP sample at 600 ºC during different annealing times: (a) 30 s, (b) 180 s, (c) 1620 s, (d) and (e) 43740 s, IPF and IQ respectively. Rolling direction (RD) and normal direction (ND). Step size of 0.02 µm.

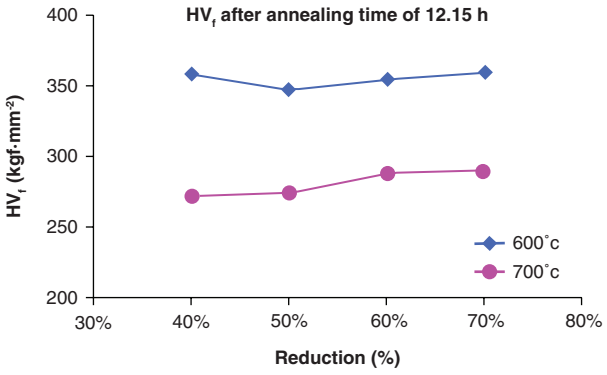

FIGURE 4. Influence of the cold rolled reduction, R, in the recrystallized grain size at 600 ºC and 700 ºC. TWIP steel.

3.2. Precipitation during isothermal annealing treatments of cold rolled TWIP steel

The effect of annealing treatments on the precipitation behavior of 60% cold rolled TWIP steel was study in the interval of temperatures 600 °C ≤ T ≤ 900 °C at long soaking time, approaching equilibrium conditions. In Table 2 are reported the annealing treatments.

3.2.1. Annealing in the range 800 °C ≤ T ≤ 900 °C

In Fig. 5 are shown the typical microstructures found for cold rolled 60% TWIP steel after soaking at 800 °C and 900 ºC. As it can be noted no

precipitation was observed by SEM analysis. Only oxide particles and *MnS* were detected. In addition, in the thermodynamic study, the isothermal section of Fe-Mn-C system performed by Thermo-Calc (TCFe6 database) under the defined conditions of temperature at equilibrium did not reveal the precipitation of carbides.

3.2.2. Annealing in the range 600 °C ≤ T ≤ 700 °C

In Fig. 6a is shown a SEM image of carbides precipitated on the austenitic grain boundaries of cold rolled 60% TWIP steel after a soaking at 700 °C. The semi-quantitative analysis SEM - EDS gave a *C* content of about 7%wt consistent with carbide of cementite type. In a similar manner, in Fig. 6b is shown carbide precipitated on austenitic grain boundaries at 600 °C.

TABLE 2. Annealing treatments for precipitation study

Annealing Treatments	
Soaking Temperature (ºC)	**Soaking Time (s)**
500	36000
600	36000
700	36000
800	36000
900	36000

- Extraction replica analysis by TEM

Owing to the detection of carbide precipitation via SEM–EDS analyses, in the cold rolled samples subjected to annealing treatments at 600 °C and 700 °C further investigation was performed by using TEM observations. The replica extractions were carried out on both TWIP steel samples soaked at 600 °C and 700 °C. The precipitation features in terms of type of precipitates and chemical composition were the same. The remarkable difference was in terms of amount of precipitates since at 700 °C the number of precipitates was significantly lower than at 600 °C. The types of precipitates were: (Fe, $Mn)_3C$ – cementite and Vanadium carbo-nitrides. The presence of Vanadium carbo-nitrides is due to unwished presence of *V* in ferroalloy during ingot casting. In Fig. 7 is depicted a Vanadium carbo-nitride image characterized by fine size (< 50 nm) and its relevant diffraction pattern having a FCC structure.

In a similar manner, in Fig. 8 is reported a (Fe, $Mn)_3C$ – cementite with the relevant diffraction pattern having an orthorhombic crystal structure.

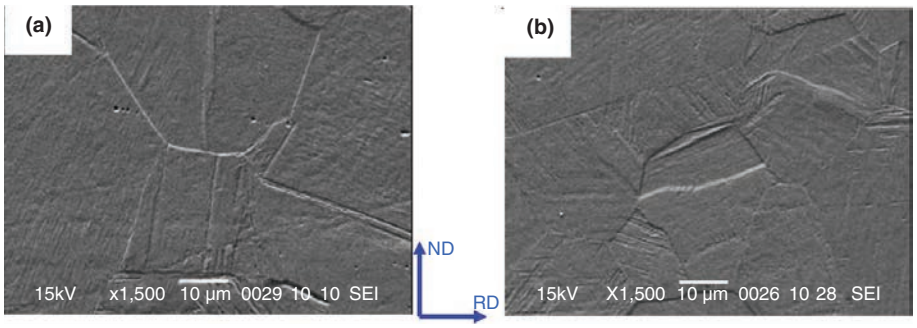

FIGURE 5. Microstructures found for TWIP steel after a soaking at (a) 800 °C and (b) 900 °C. Rolling direction (RD) and normal direction (ND).

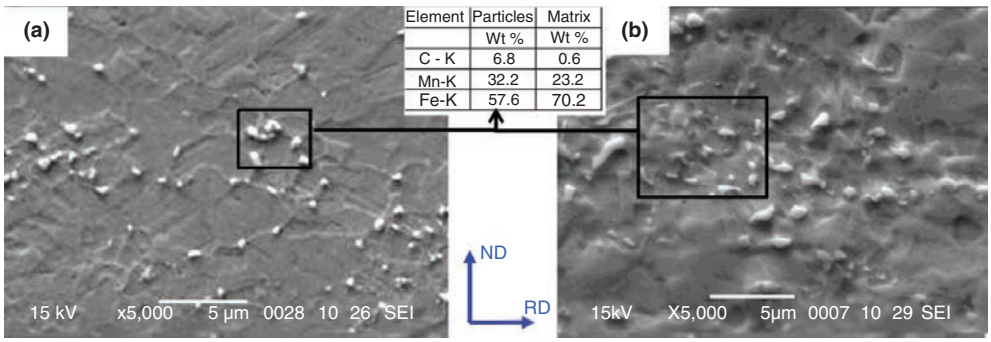

FIGURE 6. Carbides precipitates located on the austenitic grain boundaries of cold rolled 60% TWIP steel after a soaking at (a) 700 °C and (b) 600 °C.

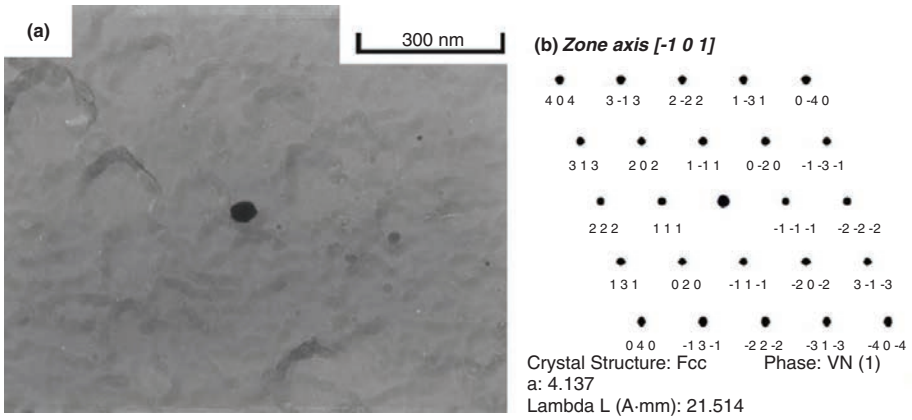

FIGURE 7. Vanadium carbo-nitrides image with its diffraction pattern, TEM image.

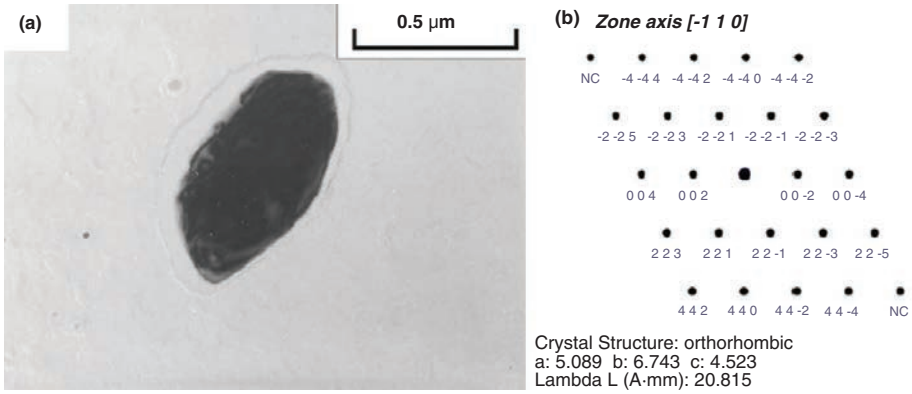

FIGURE 8. $(Fe, Mn)_3C$ – cementite image with its diffraction pattern, TEM image.

Finally, the ternary system Fe-Mn-C was assessed by means of Thermo-calc (TCFe6 database) under the defined conditions: at temperature below 700 ºC and for *Mn* content in the range 16% ≤ *Mn* %wt ≤ 22% and *C* content 0.4% ≤ C %wt ≤ 0.6% the most stable carbide is $(Fe, Mn)_3C$ cementite type with *C* content about 7%.

3.3. Textural evolution of isothermal treatments of cold rolled TWIP steel

In order to assess the textural evolution of cold rolled 60% TWIP steel in both recrystallized and recrystallized plus grain growth stages, X-ray macro-texture measurements were performed. Figure 9 illustrates the ODFs φ_2 sections (45º, 65º and 90º) of 60% cold rolled structure and recrystallized structure (without apparent grain growth). Figure 10 shows the same in recrystallized plus grain growth structure of TWIP steel for two grain sizes of structure. Recrystallized structure corresponds to 1.50 ± 0.02 μm of grain size. Recrystallized plus grain growth structures correspond to 12.2 ± 0.3 μm and 35 ± 1 μm.

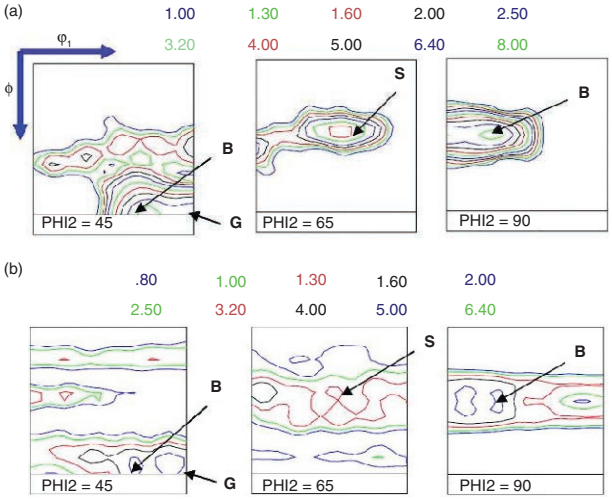

FIGURE 9. φ_2 (45º, 65º and 90º) sections of de ODFs, TWIP steel: (a) Cold rolled 60%, and (b) recrystallized grain size of D_0 = 1.50 ± 0.02 μm. φ_2=45º, Brass and Goss texture, φ_2=65º, S texture and φ_2=90º, Brass texture.

After completion of recrystallization, Fig. 9b, the main components of the rolling texture (Fig. 9a), Brass, Goss and S, remain but with much

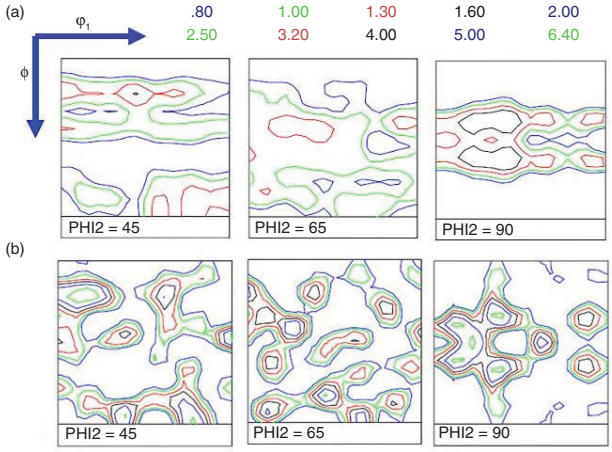

FIGURE 10. φ_2 (45º, 65º and 90º) sections of de ODFs of the cold rolled 60% TWIP alloy subjected to different annealing treatments. Recrystallized grain size of: (a) 12.2 ± 0.3 μm, and (b) 35 ± 1 μm.

weaker intensity levels. However, grain growth induces progressive qualitative texture changes. The intensity of the texture is weak, with maxima of about 2.5 random but the Brass and Goss components disappear and, different components built a new, more complicated texture, as it is evident in Fig. 10. This behaviour was observed before, De las Cuevas *et al.* (2010b), for cold rolled TWIP steel 22%Mn-0.6%C of smaller grain size (until ~ 9 μm) and other TWIP steel compositions: (I-600-011 (22.27%Mn-0.19%Si-0.5%C-0.011%N) and L-500-081 (22.7%Mn-0.21%Si-0.5%C-0.081%N)), Bracke *et al.* (2009), and Fe-30Mn-3Si-3Al, Vercammen *et al.* (2004) with similar grain growth structure.

4. DISCUSSION

4.1. Modelling of recrystallization behavior of TWIP steel

Due to the EBSP-OIM results together with the evolution of hardness with the annealing treatment (sigmoidal evolution of hardness with time), annealing treatments at 600 ºC, 650 ºC and 700 ºC were selected in order to study the kinetics of recrystallisation. The time evolution of the fraction of recrystallized, X_{soft} material for the four reductions and annealing temperatures were modelled by a Johnson-Mehl-Avrami-Kolmagorov (JMAK) type curve (Avrami, 1939; Johnson and Mehl, 1939) as it is shown in Eq. (1).

$$X_{soft}(t) = 1 - e^{-B \cdot t^{k_{soft}}} \quad (1)$$

Where k_{soft} is the time exponent. For austenite recrystallisation this time exponent is only 3 or 4, as JMAK theory predicts, in some lightly deformed fine-grained texture-free Fe-C-Mn steel grades of a uniform grain size. Most often this exponent takes values of the order of 1 for the various Fe-C-Mn steel grades (Humphreys and Hatherly, 2004; Luo *et al.*, 2004). In general, this exponent is related to the geometry of the transformation. However, according to bibliography, the geometry of transformation cannot always be deduced from the value of the exponent, k_{soft} (Doherty *et al.*, 1997; Humphreys and Hatherly, 2004; Luo *et al.*, 2004).

B, which accepts an Arrhenius expression described by Eq. (2) is a factor containing the activation energy for recystallisation, Q_{soft}. In general, this value contains all the temperature dependent terms because thermal activation affects the growth strongly through boundary/interface mobility, and therefore the nucleation density depends very strongly on driving force.

$$B = B_0 \cdot \exp\left(-\frac{Q_{soft}}{RT}\right) \quad (2)$$

B_0 depends on the chemical composition of the cold rolled TWIP steel.

In order to obtain the parameters of JMAK equation (k_{soft} and *B*), linear regressions between $\ln\left[\ln\left(\frac{1}{1-X_{soft}}\right)\right]$ against $\ln(t)$ have been made in the Eq. (3).

$$\ln\left[\ln\left(\frac{1}{1-X_{soft}}\right)\right] = k_{soft} \cdot \ln(t) + \ln(B) \quad (3)$$

The calculated time exponents for TWIP steel range from 0.8 to 0.3, with some trend to decrease as the recrystallisation temperature increases (De las Cuevas *et al.*, 2010b).

Figure 11a illustrates the softening fitting at 600 ºC for 40%, 50%, 60% and 70% reductions. The beginning of recrystallisation is practically the same for the four reductions. However, owing to the stored free energy of high cold rolled TWIP steel (60% and 70%) less time is taken for ending the recrystallisation process as it is demonstrated by the different gradients of green and pink (70% and 60% respectively) curves compared with blue and red slopes (40% and 50% respectively). Figure 11b shows the same evolution of static recrystallisation as a function of time at 700 ºC. As it can be observed at 700 ºC more clearly than at 600 ºC, the greater the deformed material (60% and 70%), the more free energy is stored in the material, therefore less time is taken to complete the recrystallisation process. Figure 11c depicts for 60% cold rolled TWIP

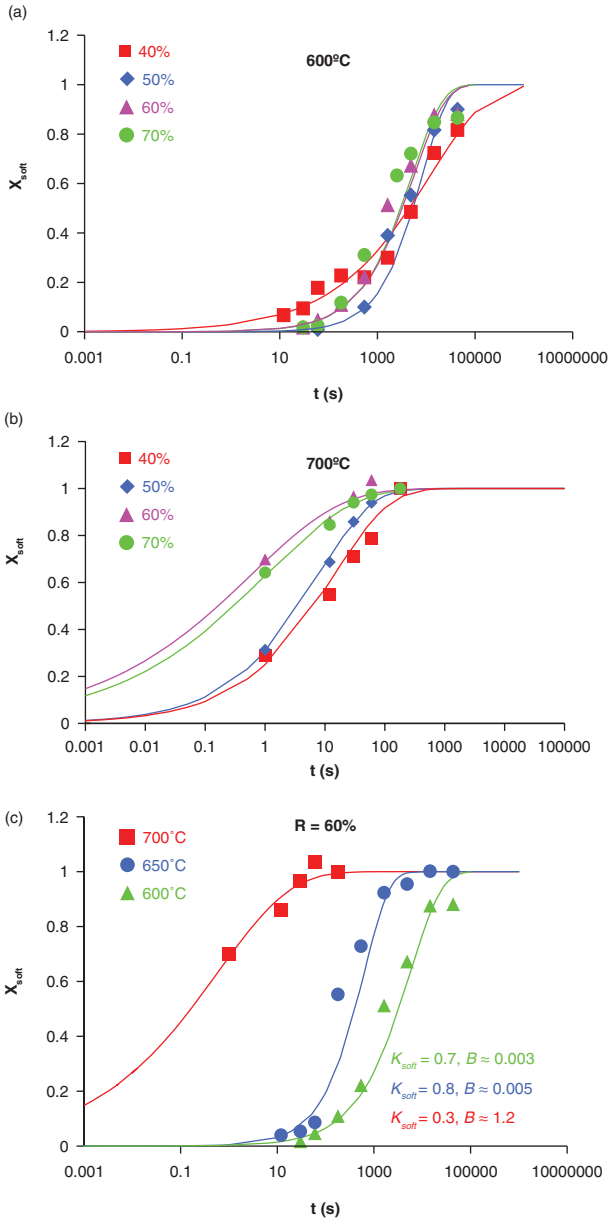

FIGURE 11. Softened fraction as a function of annealing time for 40%, 50%, 60% and 70% reductions at two temperatures: (a) 600 ºC and (b) 700 ºC, (c) softened fraction as a function of annealing time for R = 60% at 600 ºC, 650 ºC and 700 ºC TWIP steel.

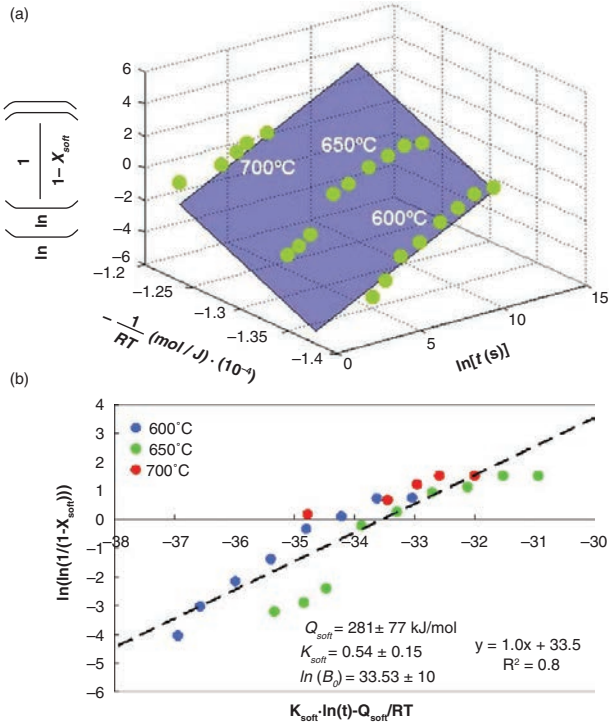

FIGURE 12. Refined characterisation of the JMAK type curves for 60% reduction TWIP steel derived from the softening by annealing at 600 ºC, 650 ºC and 700 ºC: (a) plane fitted to experimental points, and (b) optimised K_{soft}, Q_{soft} and $ln\ (B_0)$ values obtained from the polynomial regression.

the same representation at 600 ºC, 650 ºC and 700 ºC. Clearly, at higher temperatures (700 ºC), faster recrystallisation process takes place.

Although the time to reach the practical end of recrystallisation is very small above 650 ºC and the recrystallised grain size is so small as well (D_0 = 1.50 ± 0.02 μm in all cases), a further intent at a refined characterisation of the kinetic equation of recrystallisation for 60% cold rolled TWIP steel was performed. Taking into account the multiple linear Eq. (5.4), a plane has been fitted to experimental points (softened fraction at 600 ºC, 650 ºC and 700 ºC) optimising the square of the correlation index, R^2 as it is shown in Fig. 12a. The coefficients of polynomial regression are $\boldsymbol{k_{soft}}$ and Q_{soft}, and lnB_0 corresponds to an independent term as it is depicted in Fig. 12b. Reasonable values of k_{soft} and Q_{soft} have been obtained respectively, 0.54 ± 0.15 and 281 ± 70 kJ·mol^{-1} where the activation energy for recrystallisation corresponds practically with the activation energy for bulk self-diffusion in austenite, 270 kJ·mol^{-1}, Humphreys and Hatherly (2004), and for *Mn* diffusion in the austenite lattice, 265 kJ·mol^{-1} (Sun and Pugh, 2000). This is in accordance with Scott *et al.* (2006) who found Q_{soft} ~ 300 kJ·mol^{-1} for the same TWIP steel but for a cold rolled reduction of 50%.

4.2. Modelling of grain growth kinetics behavior of TWIP steel

Once recrystallization is complete the new grain structure starts to grow. The result is a new strain-free polycrystalline structure with a Gibbs free energy much lower than the energy of the deformed state (Humphreys and Hatherly, 2004).

The kinetics of grain growth was characterized via empirical equation Eq. (4) (Burke and Turnbull, 1952):

$$D^{nGG} - D_0^{nGG} = K_{GG} \cdot t \qquad (4)$$

Where D is the mean grain size after a growth time t, starting the growth from a mean grain size D_0. The grain growth exponent n_{GG} theoretically takes the value of 2 (Burke and Turnbull, 1952): The factor K_{GG} follows the Arrhenius form (Eq. (5)):

$$K_{GG} = (K_{GG})_0 \cdot \exp\left(-\frac{Q_{GG}}{RT}\right) \quad (5)$$

Where Q_{GG} is the activation energy for grain growth, and $(K_{GG})_0$ a pre-exponential constant. Owing to the small recrystallised grain size as demonstrated in the EBSP-OIM measurements ($D_0 = 1.50 \pm 0.02$ μm), Eq. (4) leads to the following approximation (Eq. (6)):

$$D^{n_{GG}} \approx K_{GG} \cdot t = \left[(K_{GG})_0 \cdot \exp\left(-\frac{Q_{GG}}{RT}\right)\right] \cdot t \quad (6)$$

Combining all the data from annealing treatments in the temperature range of 800 ºC ≤ T ≤ 1100 ºC and annealing times ranging from 12 s ≤ t ≤ 43740 s, which correspond to grain growth stage for TWIP steel, a good linear fitting is obtained using Eq. (7) where the slope of the linear fit is the time exponent n_{GG}.

$$\ln\left[t \cdot \exp\left(-\frac{Q_{GG}}{RT}\right)\right] = n_{GG} \cdot \ln(D) - \ln(k_{GG})_0 \quad (7)$$

The grain growth equation has been optimised using numerical methods that maximize the square of the correlation index, R^2. The values Q_{GG} and n_{GG} that optimise R^2 in the linear regression are respectively 384 ± 60 kJ·mol^{-1} and 4.05 ± 0.80. By using Student's t-distribution, the dashed black line in Fig. 13 corresponds to the confidence interval of the slope n_{GG} of the linear regression, whilst the dashed blue lines represent the confidence interval of the population of experimental data (blue points).

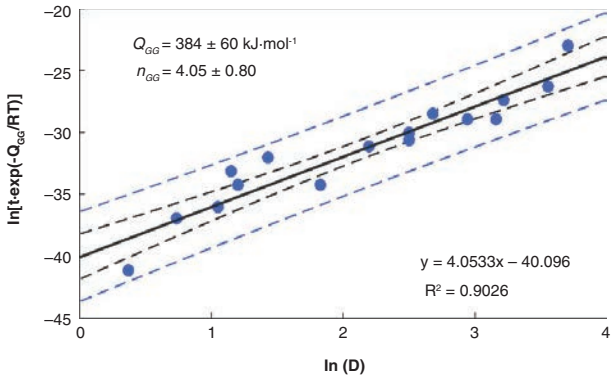

FIGURE 13. Optimised grain growth equation. D is calculated using mean linear intercept method, twin boundaries counted as grain boundaries.

Values of n_{GG} larger than two indicate a *grain boundary drag process* associated with inclusions, carbides or chemical segregation (solute drag) at the boundaries (German, 1978; Humphreys and Hatherly, 2004). An exponent other than two means a nonlinear dependence of grain boundary velocity on driving pressure (Burke and Turnbull, 1952). Values of n_{GG} equals to 2 are rarely found experimentally even in very pure materials and average values are close to 2.4. The larger measured exponents, n_{GG}, are a consequence of the materials used not being ideal (high purity metals) i.e. not consistent with the basic assumptions about the material which are incorporated in the models (Humphreys and Hatherly, 2004).

In the case of medium carbon TWIP steel (22%Mn-0.6%C), at temperature range of 600 ºC ≤ T ≤ 700 ºC the recrystallised grain size is very fine ($D_0 = 1.50 \pm 0.02$ μm) and equiaxed, the textures of recrystallisation and grain growth are very weak and it was found carbide precipitation of (Fe, Mn)$_3$C–cementite and Vanadium carbonitrides on the austenite grain boundaries. Concerning, the activation energy of TWIP steel for recrystallisation (281 ± 77 kJ·mol^{-1}), it is pointed out that it copes with both the activation energy for self-diffusion in austenite, 270 kJ·mol^{-1}, (Humphreys and Hatherly, 2004), and for *Mn* diffusion in the austenite lattice, 265 kJ·mol^{-1} (Sun and Pugh, 2000). It clearly implies that at 600 ºC and 700 ºC where carbide precipitation takes place, the effect of *grain boundary drag* by the very fine precipitates does not have an important effect. Therefore, one possibility is that the quantity of precipitates is not enough to have a relevant pinning effect. In addition, the distribution of precipitates at such temperatures could be very dispersed where the mean length between precipitates, L_{prec}, is larger than or equal to the recrystallised grain size, D_0 (neglected grain growth), $L_{prec} \geq D_0$ as it is depicted in Fig. 14a. Nevertheless, the activation energy for grain growth is found to be much higher (384 ± 60 kJ·mol^{-1}) than for recrystallisation process. The reason for such difference is believed to be associated to *grain boundary drag* (pinning of migrating grain boundaries by precipitates) being only effective for grain sizes above some threshold value, $D_{threshold}$. For the vanadium carbides to dissolve, the temperature of heating for quenching should be at least 1150 ºC in austenitic steels with high *Mn* content (Kalashnikov *et al.*, 2001). In our case, annealing treatments were performed up to 1100 ºC. Therefore, the most plausible explanation is that the quantity of precipitates is enough to have relevant *grain boundary drag* during grain growth because the mean length between precipitates, L_{prec}, is smaller than some threshold value of grain size,

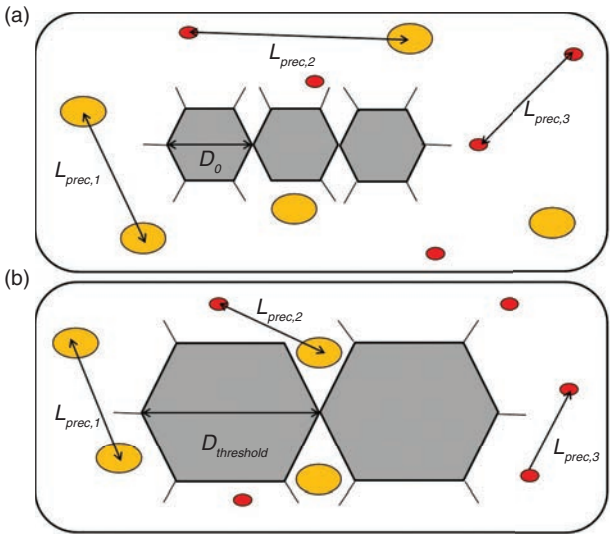

FIGURE 14. Schematic model for the influence of precipitates in (a) recrystallization process and (b) grain growth process for TWIP steel. Red ovals correspond to Vanadium carbo-nitrides and orange ovals represent (Fe, Mn)$_3$C – cementite. $L_{prec,1}$, $L_{prec,2}$ *and* $L_{prec,3}$ are the mean length between precipitates of the same type or different type. The recrystallised grain size is D_0 and grain size after some grain growth $D_{threshold}$ is a grain size where pinning of migrating grain boundaries by carbides or vanadium carbo-nitrides are effective.

$L_{prec} < D_{threshold}$, being the recrystallised grain size smaller than the grain size after some grain growth, $D_{threshold} >> D_0$ as it is described in Fig. 14b.

4.3. Texture development during recrystallization and grain growth, and their mechanisms

The results strongly induce to conclude that the factor controlling the recrystallisation behaviour and the final microstructure of TWIP steels is the nucleation. One of the main reasons for the very small size of the grains after completion of recrystallisation is most likely due to the availability of many nucleation sites because of the tremendous number of mechanical twin intersections after 60% cold rolling deformation. Furthermore, the apparent homogeneity of the deformation structure does not provide any preferred nucleation site. Hence, the nucleation events may occur in a randomly dispersed manner throughout the deformed austenitic matrix which is confirmed by the EBSP-OIM images illustrated in Fig. 3. It is noticed that very small recrystallised grain sizes of austenitic stainless steel (metastable austenite) and TWIP steels had previously been reported (Vercammen *et al.,* 2004; Bracke *et al.,* 2009).

In this research work, as the same components are found in the cold rolled texture and in the recrystallised texture, the nuclei formed should have the same orientation distribution than the deformation texture. This clearly points against oriented nucleation. Besides the grain size change, the only concomitant structural change that occurs in grain growth is the increasing presence of recrystallized twin boundaries with respect to the recrystallized structure. That means an increased volume fraction of recrystallized twin variants of the original components of the texture (De las Cuevas *et al.*, 2010b). Only extensive grain growth promotes the emergence of new orientations of very low intensity (Vercammen *et al.,* 2004; Bracke *et al.,* 2009).

It is well known that recovery processes are difficult in low-SFE materials, and thus the driving force for recrystallisation is higher than in high-SFE materials such as Al (Hurley and Humphreys, 2003a; Hurley and Humphreys, 2003b). This condition may account for the near site-saturated character of the nucleation process in TWIP steels. Furthermore, the retained rolling texture in the recrystallisation process, as well as the homogeneous nature of deformation structure, which implies the nucleation without any preferred orientation mechanism and thus inhibits a sequential spread of nucleation events, also contributes to a very high nucleation rate at the onset of recrystallisation. The limited growth rate observed in our experiments before the end of complete recrystallisation can be attributed as a consequence of the profuse near site-saturated character of the nucleation and the ensuing impingement of growing grains soon after their nucleation.

5. CONCLUSIONS

The main conclusions of this research work concerning the 22% Mn-0.6% (% in mass) TWIP steel are:

- The precipitation behavior of TWIP steel depends on one side on the *C*, *N*, and elements carbide-nitride formers (Ti, Al, Nb, V) content, but on the other side is strongly affected by thermodynamically stability of austenite in the range 600 °C ≤ T ≤ 700 °C. It was found via extraction replica for TEM observations that precipitation of (Fe, Mn)$_3$C–cementite and Vanadium carbonitrides occur on the austenite grain boundaries. Qualitatively a massive precipitates happens at 600 ºC, being less abundant at 700 ºC.
- The activation energy of TWIP steel for recrystallisation (281 ± 77 kJ·mol^{-1}) matches the activation energy for self-diffusion in austenite or for *Mn* diffusion in the austenite lattice (270 kJ·mol^{-1} and 265 kJ·mol^{-1} respectively). The activation energy for grain growth is found to be much higher (384 ± 60 kJ·mol^{-1}) with a grain growth exponent of $n_{GG} \sim 4$. The reason for such difference is believed to be associated to the pinning of migrating grain boundaries by

carbides or vanadium carbo-nitrides being only effective for grain sizes above some threshold value larger than the recrystallised grain size, $D_{threshold} >> D_0$.

– Quantitatively, recrystallization and recrystallization plus grain growth strongly weaken the texture. Consequently, the elastic and plastic anisotropies of the annealed sheets will be small, i.e. there are few possibilities of exploiting the plastic anisotropy of TWIP sheet for forming sheets or for texture strengthening. In addition, it is reasonable to explain that the nucleation events occur in a randomly dispersed manner throughout the deformed austenite matrix. This clearly points in the direction of nucleation without any preferred orientation. Only after prolonged grain growth new texture components are detected.

ACKNOWLEDGEMENTS

Economical support from the European Union, Research Programme of the Research Fund for Coal and Steel (contract RFSR-CT-00030) and from the Spanish Ministry of Science and Innovation (action MAT2005-23927-E). We would like to thank D. Badiola for their scientific support in this research work. Finally, I would like to show my deep appreciation to Jerónimo, Martín, Claudia y Pachi.

REFERENCES

Allain, S., Chateau, J.-P., Bouaziz, O., Migot, S., Guelton, N. (2004). Correlations between the calculated stacking fault energy and the plasticity mechanisms in Fe–Mn–C alloys. *Mat. Sci. Eng. A* 387–389, 158–162. https://doi.org/10.1016/j.msea.2004.01.059.

Avrami, M. (1939). Kinetics of phase change I – General theory. *J. Chem. Phys.* 7 (12), 1103–1112. https://doi.org/10.1063/1.1750380.

Bouaziz, O., Allain S., Scott, C. (2008). Effect of grain and twin boundaries on the hardening mechanisms of twinning-induced plasticity steels. *Scripta Mater.* 58 (6), 484–487. https://doi.org/10.1016/j.scriptamat.2007.10.050.

Bouaziz, O., Allain S., Scott, C.P., Cugy, P., Barbier, D. (2011). High manganese austenitic twinning induced plasticity steels: A review of the microstructure properties relationships. *Curr. Opin. Solid St. M. Sci.* 15 (4), 141–168. https://doi.org/10.1016/j.cossms.2011.04.002.

Bracke, L., Verbeken, K., Kestens, L., Penning, J. (2009). Microstructure and texture evolution during cold rolling and annealing of a high Mn TWIP steel. *Acta Mater*. 57 (5), 1512–1524. https://doi.org/10.1016/j.actamat.2008.11.036.

Burke, J.E., Turnbull, D. (1952). Recrystallization and grain growth. *Prog. Met. Phys.* 3, 220–292. https://doi.org/10.1016/0502-8205(52)90009-9.

Chen, L., Zhao, Y., Qin, X. (2013). Some Aspects of High Manganese Twinning-Induced Plasticity (TWIP) Steel, A Review. *Acta Metall. Sin.* 26 (1), 1–15. https://doi.org/10.1007/s40195-012-0501-x.

Cornette, D., Cugy, P., Hildenbrand, A., Bouzekri, M., Lovato, G. (2005). Ultra high strength FeMn TWIP steels for automotive safety parts. *Rev. Met. Paris* 102 (12), 905–918. https://doi.org/10.1051/metal:2005151.

De Cooman, B.C., Chin, K.-G., Kim, J.M. (2011). *New Trends and Developments in Automotive System Engineering*. *High Mn TWIP Steels for Automotive Applications*. Chapter 6, Editor Marcello Chiaberge, IntechOpen.

De las Cuevas, F., Reis, M., Ferraiuolo, A., Pratolongo, G., Karjalainen, L.P., Alkorta, J., Gil Sevillano, J. (2010a). Hall-Petch relationship of a TWIP steel. *Key Eng. Mater.* 423, 147–152. https://doi.org/10.4028/www.scientific.net/KEM.423.147.

De las Cuevas, F., Reis, M., Ferraiuolo, A., Pratolongo, G., Karjalainen, L.P., García Navas, V., Gil Sevillano, J. (2010b). Kinetics of recrystallization and grain growth of cold rolled TWIP steel. *Adv. Mat. Res.* 89–91, 153–158. https://doi.org/10.4028/www.scientific.net/AMR.89-91.153.

De las Cuevas, F., Ferraiuolo, A., Karjalainen, L.P., Gil Sevillano, J. (2014). Propiedades mecánicas a tracción de un acero TWIP a altas velocidades de deformación: relación de Hall-Petch. *Rev. Metal.* 50 (4), e031. https://doi.org/10.3989/revmetalm.031.

De las Cuevas, F., Gil Sevillano, J. (2017). Loss of ductility due to decarburation and Mn depletion of a coarse-grained TWIP steel. *Rev. Metal.* 53 (4), e109. https://doi.org/10.3989/revmetalm.109.

Doherty, R.D., Hughes, D.A., Humphreys, F.J, Jonas, J.J., Juul Jensen, D., Kassner, M.E., King, W.E., McNelley, T.R., McQueen, H.J., Rollet, A.D. (1997). Current issues in recrystallization: a review. *Mat. Sci. Eng. A* 238 (2), 219–274. https://doi.org/10.1016/S0921-5093(97)00424-3.

Dumay, A., Chateau J.-P., Allain, S., Migot, S., Bouaziz, O. (2008). Influence of addition elements on the stacking-fault energy and mechanical properties of an austenitic Fe-Mn-C steel. *Mat. Sci. Eng. A* 483–484, 184–187. https://doi.org/10.1016/j.msea.2006.12.170.

Frommeyer, G., Grässel, O. (1998). Light Constructional Steel and the Use Thereof. Patent PCT/EP98/04044. WO 99/01585Al.

Frommeyer, G., Drewes, E.J., Engl, B. (2000). Physical and mechanical properties of iron-aluminium- (Mn, Si) light-weight steels. *Rev. Met. Paris* 97 (10), 1245–1253. https://doi.org/10.1051/metal:2000110.

Galán, J., Samek, L., Verleysen, P., Verbeken, K., Houbaert, Y. (2012). Advanced high strength steels for automotive industry. *Rev. Metal.* 48 (2), 118–131. https://doi.org/10.3989/revmetalm.1158.

German, R.M. (1978). Grain growth in austenitic stainless steels. *Metallography* 11 (12), 235–239. https://doi.org/10.1016/0026-0800(78)90043-5.

Ghasri-Khouzani, M., McDermid, J.R. (2015). Effect of carbon content on the mechanical properties and microstructural evolution of Fe-22Mn-C steels. *Mat. Sci. Eng. A* 621, 118–127. https://doi.org/10.1016/j.msea.2014.10.042.

Grässel, O., Frommeyer, G, Derder, C., Hofmann, H. (1997). Phase transformation and mechanical properties of Fe-Mn-Si-Al TRIP-steels. *J. Phys. IV France* 7 (C5), 383–388. https://doi.org/10.1051/jp4:1997560.

Grässel, O., Frommeyer, G. (1998). Effect of martensitic phase transformation and deformation twinning on mechanical properties of Fe-Mn-Si-Al steels. *Mater. Sci. Tech.* 14 (12), 1213–1217. https://doi.org/10.1179/mst.1998.14.12.1213.

Grässel, O., Krüger, L., Frommeyer, G., Meyer, L.W. (2000). High strength Fe-Mn-(Al, Si) TRIP/TWIP steels development - properties - application. *Int. J. Plasticity* 16 (10–11), 1391–1409. https://doi.org/10.1016/S0749-6419(00)00015-2.

Gil Sevillano, J., de las Cuevas, F. (2012). Internal stresses and the mechanism of work hardening in twinning-induced plasticity steels. *Scripta Mater.* 66 (12), 978–981. https://doi.org/10.1016/j.scriptamat.2012.02.019.

Hamada, A.S., Karjalainen, L.P., Ferrraiuolo, A., Gil Sevillano, J., de las Cuevas, F., Pratolongo, G., Reis, M. (2010). Fatigue behavior of four high-Mn twinning induces plasticity effect steels. *Metall. Mater. Trans. A* 41 (5), 1102–1108. https://doi.org/10.1007/s11661-010-0193-7.

Humphreys, F.J., Hatherly, M. (2004). *Recrystallization and related annealing phenomena*. 2nd Edition, Elsevier Ltd, Oxford, England.

Hurley, P.J., Humphreys, F.J. (2003a). The application of EBSD to the study of substructural development in a cold rolled single-phase aluminium alloy. *Acta Mater.* 51 (4), 1087–1102. https://doi.org/10.1016/S1359-6454(02)00513-X.

Hurley, P.J., Humphreys, F.J. (2003b). Modelling the recrystallization of single-phase aluminium. *Acta Mater.* 51 (13), 3779–3793. https://doi.org/10.1016/S1359-6454(03)00192-7.

Johnson, W.A., Mehl, R.F. (1939). Reaction kinetics in processes of nucleation and growth. *Transactions of the AIME* 135, 416–458.

Kalashnilov, I.S., Ermakov, B.S., Aksel´rad, O., Pereira, L.K. (2001). Alloying of steels of the Fe-Mn-Al-C system with refractory elements. *Met. Sci. Heat Treat.* 43 (11–12), 493–496. https://doi.org/10.1023/A:1014805123438.

Leslie, W.C., Rauch, G.C. (1978). Precipitation of carbides in low-carbon Fe-Al-C alloys. *Metall. Trans. A* 9 (3), 343–349. https://doi.org/10.1007/BF02646383.

Luo, H., Sietsma, J., Van Der Zwaag, S. (2004). A metallurgical interpretation of the static recrystallization kinetics of an intercritically deformed C-Mn steel. *Metall. Mater. Trans. A* 35 (6), 1889–1898. https://doi.org/10.1007/s11661-004-0097-5.

Marder A.R. (1989). *ASM Handbook: Nondestructive evaluation and quality control*. Vol. 17, ASTM International, USA.

Pierce, D.T., Jiménez, J.A, Bentley, J., Raabe, D., Oskay, C., Witting, J.E. (2014). The influence of manganese content on the stacking fault and austenite / e-martensite interfacial energies in Fe-Mn-(Al-Si) steels investigated by experiment and theory. *Acta Mater.* 68, 238–253. https://doi.org/10.1016/j.actamat.2014.01.001.

Pierce, D.T., Jiménez, J.A, Bentley, J., Raabe, D., Oskay, C. Witting, J.E. (2015). The influence of stacking fault energy on the microstructural and strain hardening evolution of Fe–Mn–Al–Si steels during tensile deformation. *Acta Mater.* 100, 178–190. https://doi.org/10.1016/j.actamat.2015.08.030.

Scott C., Allain S., Faral, M., Guelton, N. (2006). The development of a new Fe-Mn-C austenitic steel for automotive applications. *Rev. Met. Paris* 103 (6), 293–302. https://doi.org/10.1051/metal:2006142.

Schramm, R.E., Reed, R.P. (1975). Stacking-fault energies of 7 commercial austenitic stainless-steels. *Metall. Trans. A-Phys. Metall. Trans. A* 6 (7), 1345–1351. https://doi.org/10.1007/BF02641927.

Sun, S., Pugh, M. (2000). Manganese partitioning in dual-phase steel during annealing. *Mat. Sci. Eng. A-Struct.* 276 (1–2), 167–174. https://doi.org/10.1016/S0921-5093(99)00261-0.

Vercammen, S., Blanpain, B., De Cooman, B.C., Wollants, P. (2004). Cold rolling behaviour of an austenitic Fe–30Mn–3Al–3Si TWIP-steel: the importance of deformation twinning. *Acta Mater*. 52 (7), 2005–2012. https://doi.org/10.1016/j.actamat.2003.12.040.

Vidoz, A.E., Lazarevic, D.P., Cahn, R.W. (1963). Strain-ageing of ordering alloys, with special reference to Nickel-Iron system. *Acta Metall.* 11 (1), 17–33. https://doi.org/10.1016/0001-6160(63)90121-4.